Journal of the European Ceramic Society 22 (2002) 2173–2179

www.elsevier.com/locate/jeurceramsoc

Influence of alumina particle size on fracture toughness of (Y,Nb)-TZP/Al_2O_3 composites

Deuk Yong Lee[a,*], Dae-Joon Kim[b], Bae-Yeon Kim[c]

[a]*Department of Materials Engineering, Daelim College of Technology, Anyang 431-715, South Korea*
[b]*Multifunctional Ceramics Research Center, Korea Institute of Science and Technology, Seoul 136-791, South Korea*
[c]*Department of Materials Science and Engineering, University of Incheon, Incheon 402-749, South Korea*

Received 20 September 2001; received in revised form 15 December 2001; accepted 28 December 2001

Abstract

ZrO_2/Al_2O_3 composites were prepared by mixing a tetragonal ZrO_2, stabilized with 5.31 mol% Y_2O_3 and 4.45 mol% Nb_2O_5, and Al_2O_3 having different particle size (0.2 μm and 2.8 μm) to investigate the influence of the Al_2O_3 particle size on flaw tolerance of the composites. The composites exhibited rising R-curve behavior and plateau fracture toughness of 7.9 and 8.8 MPa$\sqrt{m}$ for the additions of 20 vol.% of 0.2 and 2.8 μm Al_2O_3 particles, respectively. The difference in the fracture resistance was attributed mainly to the grain size of tetragonal phase in the composites, which scaled with the Al_2O_3 particle diameter, and partially to the dispersion toughening.

Keywords: Composites; R-curve; Toughness; Al_2O_3-ZrO_2

1. Introduction

Tetragonal zirconia polycrystals (TZPs), stabilized by doping with oxides such as Y_2O_3 and CeO_2, show a rising crack growth resistance with crack extension (R-curve behavior) due to the formation of the transformation zone behind the crack tip as a result of the stress-induced phase transformation.[1–8] TZP ceramics showing R-curve behavior are considered to be more tolerant of existing processing defects and surface damage induced under in-service conditions, and thus are reliable as structural ceramics due to the narrow strength distribution. Despite the fracture resistance, TZP stabilized by alloying with 3 mol% Y_2O_3 (3Y-TZP) experiences a detrimental strength degradation because of the spontaneous tetragonal (t) to monoclinic (m) phase transformation when the material is exposed to a low-temperature range of 100 to 400 °C for a long period of time in air or water.[9] The low temperature degradation can be prevented by increasing the stabilizer content, decreasing the average grain size, or by the formation of TZP composites with Al_2O_3.[9–10] However, these solutions lead to a decrease in the fracture toughness because the stress-induced $t \rightarrow m$ phase transformation becomes suppressed.

Recently it has been reported that Nb_2O_5 and Y_2O_3 co-doped TZPs ((Y,Nb)-TZP) exhibits the low-temperature phase stability in air while maintaining a reasonably high fracture toughness of 8.1 MPa$\sqrt{m}$.[11] The absence of the degradation in (Y,Nb)-TZP under the low temperature condition is attributed to a relief of internal strain in the t-ZrO_2 lattice[12] as a result of local Y-Nb ordering in t-ZrO_2 into a scheelite-like arrangement.[13] The internal strain is known to assist the degradation under aging environments.[12] Besides, the concentration of oxygen vacancy in t-ZrO_2, created by the Y^{3+} doping, is diminished by an additional doping with Nb^{5+}, leading to a low oxygen vacancy diffusion rate that governs the $t \rightarrow m$ phase transformation during aging at low temperatures.[14,15] Although (Y,Nb)-TZP has the high phase stability and fracture toughness,[11,15,16] the biaxial strength of (Y,Nb)-TZP is determined to be about 500 MPa in the present study that is somewhat lower than that of 3Y-TZP, which is about 850 MPa.[15]

The addition of Al_2O_3 to Y-TZP produces composites with improved strength and toughness.[17–24] However, the results of Tsukuma et al.[22] and Fukuhara[23] showed

* Corresponding author. Tel.: +82-31-467-4835; fax: +82-31-467-4830.
E-mail address: dylee@daelim.ac.kr (D. Y. Lee).

0955-2219/02/$ - see front matter
PII: S0955-2219(02)00012-2

that Al_2O_3 additions to Y-TZP increased strength, but decreased toughness. The discrepancies arose from different toughness test techniques; that is, indentation tests showed a decrease in the toughness,[20–23] whereas chevron-notched beam tests showed an increase.[24] Furthermore, the mechanism for the strengthening and the toughening by the Al_2O_3 alloying has not been fully understood. Glass and Green[21] have summarized that the increase in the strength and the toughness of TZP by the Al_2O_3 addition may result from (i) phase transformation toughening, (ii) grain boundary toughening, and (iii) dispersion toughening. Thus, it is desirable to delineate the entire R-curve for the Y-TZP/ Al_2O_3 composites to understand the role of Al_2O_3 in the improvements in the mechanical properties of Y-TZP. In the present study the (Y,Nb)-TZP/Al_2O_3 composites having different Al_2O_3 particle sizes were prepared in an effort to increase strength and toughness of the monolith. R-curve behavior and mechanical reliability of the composites were evaluated.

2. Experimental procedure

Powder preparation procedure of (Y,Nb)-TZP, having the monolithic composition of 90.24 mol% ZrO_2-5.31 mol% Y_2O_3-4.45 mol% Nb_2O_5 (mixture of 85 wt.% of 89.25 mol% ZrO_2-5.75 mol% Y_2O_3-5 mol% Nb_2O_5 and 15 wt.% of 95.5 mol% ZrO_2-3 mol% Y_2O_3-1.5 mol% Nb_2O_5), was reported elsewhere.[11] (Y,Nb)-TZP/Al_2O_3 powder mixtures were prepared by adding 10, 20, and 30 vol.% of Al_2O_3 into the (Y,Nb)-TZP and ball milling in a polyethylene jar with zirconia balls for 24 h. Al_2O_3 powders (Sumitomo Chemical Co., Japan) with different average size (0.2 μm and 2.8 μm) were used as particulates. The milled slurries were dried, sieved through a 100-mesh screen, die-pressed into disks, and then isostatically pressed at 140 MPa. The green compacts were sintered for 2 h at 1550 °C in air.

The sintered density was measured by the Archimedes method, using distilled water as the immersion medium. Thermal expansion coefficient (CTE) of (Y,Nb)-TZP samples, having dimensions 8 mm in diameter and 4 mm in thickness, was measured using a dilatometer (Netzsch, Selb, Germany) in the temperature range of room temperature to 1200 °C with a heating rate of 10 °C/min. For mechanical property measurements the disk specimens were polished to a 1 μm diamond finish. The dimension of the specimens after the polishing was 18 mm in diameter and 1.8 mm in thickness. A flat-on-three-ball biaxial-fixture was used for the determinations of strength, Weibull modulus, and toughness with a stress rate of 23 MPa/s.[25] The Weibull modulus was determined using the estimator of $P=(i-0.5)/n$,[26] where P is the failure probability, i is the ith specimen in the strength ranking and n is total number of specimens tested ($n=30$). The fracture toughness (K_{IC}) was determined by the indentation-strength method.[27] A Vickers indent of 490 N was placed on the center of the tensile face of the test specimens for the toughness determination.[27] A minimum of five tests was performed for each specimen composition. For the calculation of the toughness, the hardness to modulus ratio was estimated from the measurements of the diagonal dimensions of 49 N Knoop indentations after Marshall et al.[28]

The flaw tolerance of the composites was assessed using the indentation-strength test because of its simplicity,[3,5,27,29] even though the toughness determined by the indentation-strength method does not account for the residual stresses left by the transformation zone surrounding the indent in high-toughness zirconia ceramics.[30–32] Vickers indentations were placed on the center of the tensile surface of each disk using loads ranging from 4 to 490 N for the subsequent R-curve analysis. The indentation-induced crack length, 2c, was measured with an optical microscope to determine the crack growth resistance parameter (K_R) as reported by Anstis et al.[27] A drop of silicon oil was applied to minimize moisture assisted subcritical crack growth. For each load five specimens were broken using the biaxial test fixture. The R-curve analysis was then performed by following the procedure proposed by Krause.[33]

3. Results and discussion

Flexural strength and fracture toughness of (Y,Nb)-TZP/Al_2O_3 composites containing 0–30 vol% of the fine and the coarse Al_2O_3 particles are shown in Fig. 1. Both the flexural strength and the fracture toughness rise as the Al_2O_3 content increases. The m-ZrO_2 fraction (m-ZrO_2/t-ZrO_2) on the fracture surfaces of the monolith,[34] which corresponded to 37%, decreased continuously with increasing the amount of Al_2O_3. Regardless of the Al_2O_3 particle size, the relative density of (Y,Nb)-TZP/20 vol.% Al_2O_3 composites was 5.53 g/cm^3, corresponding to 98.5% of the theoretical density. Microstructure of the composites is shown in Fig. 2. The coarser alumina particles lead to an overall coarser TZP microstructure, even at the same volume fraction, according to the Zener's relationship[35]

$$R = 4r/3f \quad (1)$$

where R is the radius of curvature of the average grain, r is the radius of the particles, and f is the volume fraction of particles. The micrograph also show interaction between the microstructure and the crack path corresponding with the extended radial cracks of 196 N Vickers indentation on the surface as shown in Fig. 2C, indicating that the composite containing 2.8 μm Al_2O_3

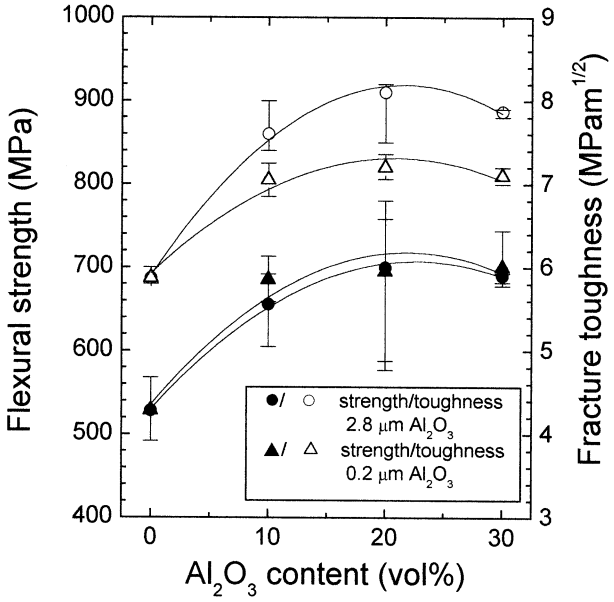

Fig. 1. Strength and fracture toughness of (Y,Nb)-TZP/Al_2O_3 composites containing different Al_2O_3 particle size as a function of Al_2O_3 content.

particles exhibits grain bridging showing incomplete separation of crack faces around Al_2O_3 particle.

The toughening by the Al_2O_3 addition may arise from toughened grain boundaries due to the segregation of aluminum impurities[21] and/or dispersion toughening that comprises the crack deflection and the grain bridging.[36] For the grain boundary toughening mechanism, the composites containing the fine Al_2O_3 should show a higher toughness than those having the coarse ones. This is because the grain boundary area and the interfaces in the former are higher than in the latter for a given fraction of Al_2O_3 in the composites as shown in Fig. 2. However, this mechanism contradicts the results in Fig. 1.

It has been suggested that the increase in the toughness by the Al_2O_3 addition is attributed to the dispersion toughening combined with a negative contribution of the transformation toughening.[36] The transformation toughening is given by[37]

$$\Delta K_c^{t\to m}(\text{phase transformation}) = k\ E\ V\ e_t\ \sqrt{h}(1-v)^{-1} \quad (2)$$

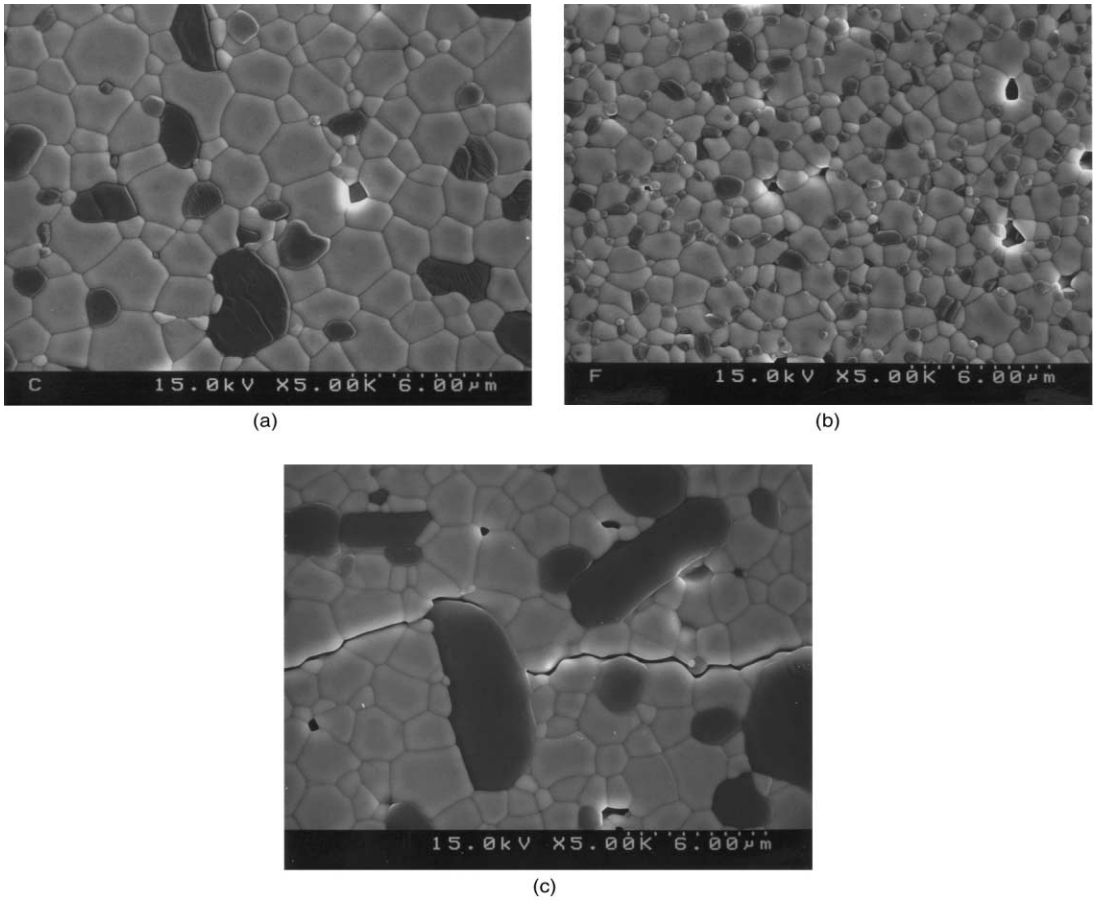

Fig. 2. Scanning electron micrographs of (a) (Y,Nb)-TZP/20 vol.% of 2.8 μm Al_2O_3 composite and (b) (Y,Nb)-TZP/20 vol.% of 0.2 μm Al_2O_3 composite and typical crack paths induced by 196 N Vickers indentation in (C) (Y,Nb)-TZP/20 vol.% of 2.8 μm Al_2O_3 composite. An intergranular crack path and grain bridging sites are apparent in Fig. 2c. Also note the influence of alumina particle size on overall TZP microstructure.

where k is a constant, E Young's modulus, V volume fraction of transformable t-ZrO_2, e_t the transformation strain, h the height of the transformation zone, ν Poisson's ratio. Li and Watanabe[36] related the influence of Al_2O_3 addition on the phase transformation to a decrease in the volume fraction of transformable t-ZrO_2. The negative contribution to toughness by decrease in V can be offset further by the increase in elastic modulus by the addition of Al_2O_3[21] and the lattice distortion in t-ZrO_2 due to the thermal expansion mismatch between the two components.[38] This leads to a residual tensile stress in the t-ZrO_2 matrix and consequently increases the transformation zone height in Eq. (2), although the zone height is somewhat reduced by grain size refinement as the Al_2O_3 content increases.[17] The Weibull distribution of the monolith and the composites containing 20 vol.% of fine and coarse Al_2O_3 particles is depicted in Fig. 3. The Weibull moduli for the monolith and the fine and the coarse Al_2O_3 containing composites are 15.1, 18.4, and 18.5, respectively, indicating that the addition of Al_2O_3 particles leads to a smaller dispersion in the size of strength-controlling flaws and the particle size does not affect significantly variation in the strength distribution of the (Y,Nb)-TZP/Al_2O_3 composites. This result also suggests that long cracks in (Y, Nb)-TZP are inhibited by the addition of Al_2O_3 particles more than short cracks so that the distribution of flaws in the monolith is effectively narrowed and the reliability is increased. It has been known that the improved Weibull modulus is resulted by R-curve behavior.[1,2,39]

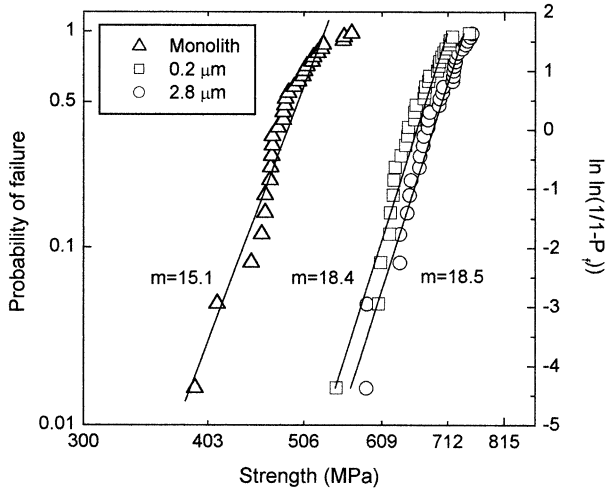

Fig. 3. Weibull plots for (Y,Nb)-TZP and (Y,Nb)-TZP/20 vol% Al_2O_3 composites having different Al_2O_3 particle sizes.

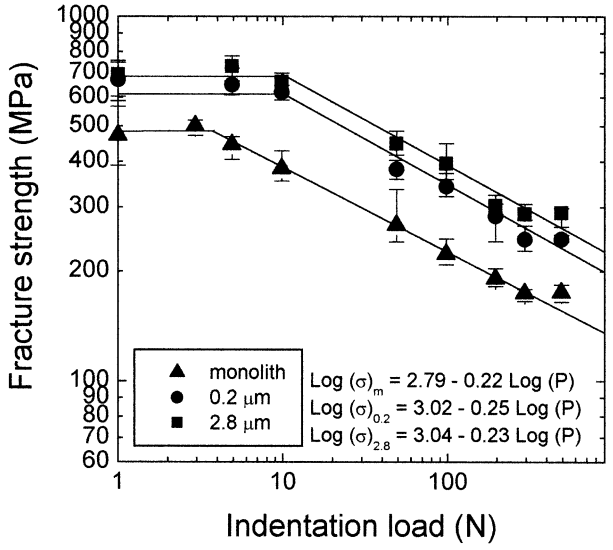

Fig. 4. Strength of (Y,Nb)-TZP and (Y,Nb)-TZP/Al_2O_3 composites as a function of indentation load. The strengths from natural flaws were arbitrarily plotted at P = 1 N.

The relationship between the strength and the indentation load of the monolith and the composites having 20 vol.% of fine and coarse Al_2O_3 particles is shown in Fig. 4. The strength from natural flaws of the monolith and the fine and the coarse Al_2O_3 containing composites was 480 MPa, 690 MPa, and 700 MPa, respectively. The strength is independent of indentation load up to about 3 N for the monolith and about 10 N for the composites. The strength starts to decrease as the load is raised above these critical loads. This shows that the unstable crack size in the composites is larger than that in the monolith and the instability crack size is not varied by the Al_2O_3 particle size. The difference in the critical loads of the monolith and the composites containing different particle size is consistent with that in the Weibull moduli in Fig. 3. Thus, it is obvious that the flaw size sensitivity of the fracture strength is related to the mechanical reliability. For all indentation loads, the strength of the composites having the coarse Al_2O_3 particles is consistently higher than that of the composites containing the fine Al_2O_3 particles possibly because of a stronger R-curve effect of the coarse particle containing composites. The linear least-squares fits of the data in Fig. 4 gave slopes smaller than 1/3 that corresponds to the slope in the conventional strength $\propto$ indentation load$^{-1/3}$ relationship for homogeneous ceramics whose fracture toughness is independent of crack extension.[32] The small slopes suggest that a rising R-curve behavior exists in both the monolith and the composites.

The R-curves of the monolith and the composites having 20 vol.% of the coarse and the fine Al_2O_3 particles were estimated from the indentation-strength data by using a power law function of K_R versus the crack extension (Δc), as suggested by Krause[33] and the results are shown in Fig. 5. The composites show more pronounced R-curve behavior than the monolith and the composites with the larger Al_2O_3 particle size exhibit a stronger R-curve effect, indicating that the fracture strength of these materials in Fig. 1 are governed by

R-curve behavior. Nevertheless, the slopes of the R-curves of the composites containing the coarse and the fine Al_2O_3 particles are not consistent with the Weibull moduli of these composites in Fig. 3.

The steady-state fracture toughness of the composites having 20 vol.% of the coarse and the fine Al_2O_3 particles are 8.8 and 7.9 MPa$\sqrt{}$m, respectively. The contribution of the Al_2O_3 particle size on the R-curve

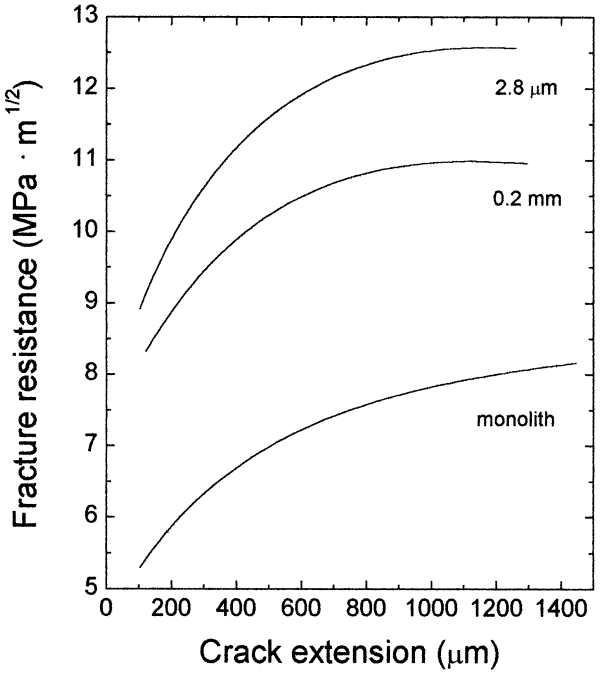

Fig. 5. R-curves for (Y,Nb)-TZP and (Y,Nb)-TZP/Al_2O_3 composites containing 20 vol% of fine and coarse Al_2O_3 particles constructed by the indentation-strength method.

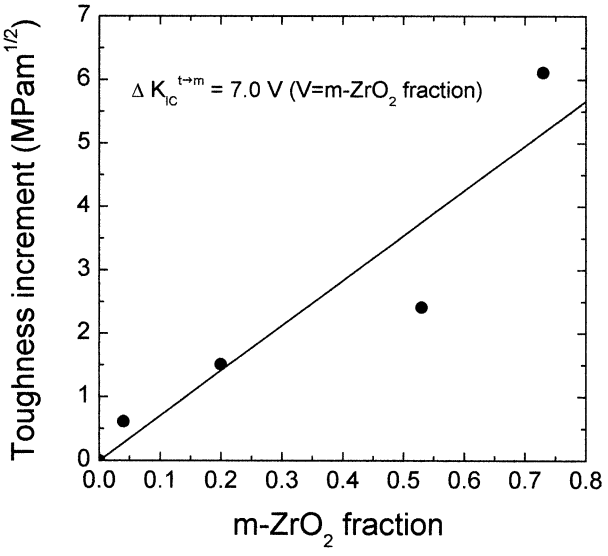

Fig. 6. Fracture toughness increment of 3Y-TZP and 3Y-TZP containing Nb_2O_5 as a function of m-ZrO_2 fraction on the fractured surface of the specimens.

behaviors of Y-TZP/Al_2O_3 composites has been related to the effects of grain bridging and thermal residual stress,[36] neglecting the particle size effect on the phase transformation. For the composites containing the coarse and the fine Al_2O_3 particles, the m-ZrO_2 content on the fracture surfaces was 30% and 22%, respectively, with an estimate of error of ±1%. The toughening increment by the phase transformation can be estimated from Eq. (2). Alternatively, the contribution of the phase transformation to the toughness increment of the composites may be calculated by measuring the fraction of m-ZrO_2 on the fracture surfaces of the (Y,Nb)-TZP/Al_2O_3 composites. This can be accomplished from the relationship between the fracture toughness increment and the m-ZrO_2 fraction on the fracture surfaces of 3Y-TZP doped with Nb_2O_5, whose doping does not influence the density and the grain size of 3Y-TZP,[13] in Fig. 6. The linear relationship is reasonable since the main contribution to the toughness in Eq. (2) is the volume fraction of transformable t-ZrO_2, especially in the case that the influence of the grain size that is directly related to the transformation zone height[40] on the toughness can be excluded. From Fig. 6 the difference in the toughness increment of the composites due to the different Al_2O_3 particle size is calculated to be about 0.6 MPa$\sqrt{}$m. The contribution of the particle size to the toughness results from the fact that the grain size of transformable t-ZrO_2 depends on the Al_2O_3 particle size according to Eq. (1). The larger the grain size, the larger the fraction of t-ZrO_2 which transforms to m-ZrO_2 since the residual stress due to the thermal expansion mismatch scales with the grain size.[41] Nevertheless, the toughness difference of 0.6 MPa$\sqrt{}$m cannot fully account for the difference in the plateau toughness values of the composites containing the fine and the coarse Al_2O_3 particles in Fig. 5, which is 0.9 MPa$\sqrt{}$m.

The discrepancy may arise from an involvement of the grain bridging in the toughness of the composites, as evidenced in Fig. 2(C), which can be calculated by[36]

$$\Delta K_c(\text{grain bridging}) = 2.5\, f\, E_p\,(\alpha_p - \alpha_m)\Delta T\sqrt{r} \qquad (3)$$

where E_p is Young's modulus of Al_2O_3 (412 GPa),[42] α_p (9.0×10^{-6}/°C)[43] and α_m (9.92×10^{-6}/°C) CTE of Al_2O_3 and (Y,Nb)-TZP, respectively, and ΔT temperature difference over which the thermal residual stresses are not relieved (1200 °C).[36] According to Eq. (3) the toughness increment by the grain bridging for the fine ($r=0.1$ μm) and the coarse ($r=1.4$ μm) Al_2O_3 is approximately 0.1 and 0.3 MPa$\sqrt{}$m, respectively, which gives the toughening difference of 0.2 MPa$\sqrt{}$m. The sum of the contributions from the phase transformation and the crack bridging is close to the toughness difference of the composites having different Al_2O_3 particle sizes. This suggests that the influence of the Al_2O_3 particle size on the toughness of (Y,Nb)-TZP comes

dominantly from enhanced phase transformation and the involvement of the grain bridging is relatively insignificant.

4. Conclusions

The (Y,Nb)-TZP mixed with the coarse Al_2O_3 particles showed a higher resistance to crack growth and thus a better flaw tolerance compared to the TZP containing the fine Al_2O_3 particles. The difference in the R-curve behaviors is largely attributed to the extent of the $t \rightarrow m$ phase transformation of the TZP whose grain size scales with the particle size. An additional contribution of the particle size to the difference arises from the more extensive grain bridging in the composites containing the coarse particles than the fine particles.

References

1. Kendall, K., Alford, N.McN., Tan, S. R. and Birchall, J. D., Influence of toughness on Weibull modulus of ceramic bend strength. *J. Mater. Res.*, 1986, **1**, 120–123.
2. Ramchandran, N., Chao, L. and Shetty, D. K., *R*-Curve behavior and flaw insensitivity of Ce-TZP/Al_2O_3 composite. *J. Am. Ceram. Soc.*, 1993, **76**, 961–969.
3. Readey, M. J. and McCallen, C. L., Microstructure, flaw tolerance, and reliability of Ce-TZP and Y-TZP ceramics. *J. Am. Ceram. Soc.*, 1995, **78**, 2769–2776.
4. Burns, S. J. and Swain, M. V., Fracture toughness of MgO-partially-stabilized ZrO_2 specimens with *R*-Curve behavior from transformation toughening. *J. Am. Ceram. Soc.*, 1986, **69**, 226–230.
5. Li, J., Kawasaki, A. and Watanabe, R., *R*-curve determination of 3Y-PSZ by the indentation strength-in-bending method. *J. Ceram. Soc. Jpn.*, 1997, **105**, 88–90.
6. Anderson, R. M. and Braun, L. M., Technique for the *R*-curve determination of Y-TZP using indentation-produced flaws. *J. Am. Ceram. Soc.*, 1990, **73**, 3059–3062.
7. Shetty, D. K. and Wang, J., Crack stability and strength distribution of ceramics that exhibit rising crack-growth-resistance (*R*-curve) behavior. *J. Am. Ceram. Soc.*, 1989, **72**, 1158–1162.
8. Yu, C. and Shetty, D. K., Transformation zone shape, size, and crack-growth-resistance (*R*-curve) behavior of ceria-partially-stabilized zirconia polycrystals. *J. Am. Ceram. Soc.*, 1989, **72**, 921–928.
9. Lawson, S., Environmental degradation of zirconia ceramics. *J. Eur. Ceram. Soc.*, 1995, **15**, 485–502.
10. Hirano, M. and Inada, H., Fabrication and properties of (Y, Ce)-TZP/Al_2O_3 and Y-TZP/Al_2O_3 composites from fine powder prepared by a hydrolysis technique. *J. Ceram. Soc. Jpn.*, 1991, **99**, 124–130.
11. Lee, D. Y., Kim, D.-J. and Cho, D.-H., Low-temperature phase stability and mechanical properties of Y_2O_3 and Nb_2O_5 co-doped tetragonal zirconia polycrystal ceramics. *J. Mater. Sci. Lett.*, 1998, **17**, 185–187.
12. Li, P., Chen, I.-W. and Penner-Hahn, J. E., Effect of dopants on zirconia stabilization-an X-ray absorption study: III, charge-compensating dopants. *J. Am. Ceram. Soc.*, 1994, **74**, 1289–1295.
13. Schmauder, S. and Schubert, H., Significance of internal stresses for the martensitic transformation in yttria-stabilized tetragonal zirconia polycrystals during degradation. *J. Am. Ceram. Soc.*, 1986, **69**, 534–540.
14. Kim, D.-J., Jung, H.-J. and Cho, D.-H., Phase transformation of Y_2O_3 and Nb_2O_5 doped tetragonal zirconia during low temperature ageing in air. *Solid State Ionics*, 1995, **80**, 67–73.
15. Kim, D.-J., Jung, H.-J., Jang, J.-W. and Lee, H.-L., Fracture toughness, ionic conductivity, and low-temperature phase stability of tetragonal zirconia co-doped with Y_2O_3 and Nb_2O_5. *J. Am. Ceram. Soc.*, 1998, **81**, 2309–2314.
16. Lee, D. Y., Jang, J.-W. and Kim, D.-J., Raman spectral characterization of existing phases in the ZrO_2-Y_2O_3-Nb_2O_5 system. *Ceram. Intl.*, 2001, **27**, 291–298.
17. Lee, D. Y., Kim, D.-J., Jang, J.-W., Choi, D.-W. and Lee, S.-J., Phase stability of (Y, Nb)-TZP/Al_2O_3 composites under low temperature hydrothermal conditions. *Mater. Lett.*, 1999, **39**, 221–226.
18. Lange, F. F., Transformation toughening, part 4, fabrication, fracture toughness, and strength of Al_2O_3-ZrO_2 composites. *J. Mater. Sci.*, 1982, **17**, 247–254.
19. Shimada, T., Nagata., K., Hashiba, M., Miura, E., Ono, T. and Nurishi, Y. *Advances in Ceramics, Vol. 24A*, S. Somiya, N. Yamamoto and H. Yanagida ed. Am. Ceram. Soc., Westerville, OH, 1988, p. 397.
20. Shi, J. L., Li, B. S. and Yen, T. S., Mechanical properties of Al_2O_3 particle-Y-TZP matrix composite and its toughening mechanism. *J. Mater. Sci.*, 1993, **28**, 4019–4022.
21. Glass, S. J. and Green, D. J., Mechanical properties of infiltrated alumina-Y-TZP composites. *J. Am. Ceram. Soc.*, 1996, **79**, 2227–2236.
22. Tsukuma, K., Takahata, T. and Shiomi, M. *Advances in Ceramics, Vol. 24A*, S. Somiya, N. Yamamoto and H. Yanagida ed. Am. Ceram. Soc., Westerville, OH, 1988, p. 397.
23. Fukuhara, M., Properties of (Y) ZrO_2-Al_2O_3 and (Y) ZrO_2-Al_2O_3-(Ti or Si)C composites. *J. Am. Ceram. Soc.*, 1989, **72**, 236–242.
24. Tsukuma, T., Ueda, K. and Shimada, M., Strength and fracture toughness of isostatically hot-pressed composites of Al_2O_3 and Y_2O_3-partially-stabilized ZrO_2. *J. Am. Ceram. Soc.*, 1985, **68**, C4–C5.
25. ASTM Standard F394–78, in ASTM Annual Book of Standards, Vol. 15.02, Section 15, American Society for Testing and Materials, Philadelphia, PA, 1996, p. 446.
26. Sullivan, J. D. and Lauzon, P. H., Experimental probability estimators for Weibull plots. *J. Mater. Sci. Lett.*, 1986, **5**, 1245–1247.
27. Anstis, G. R., Chantikul, P., Lawn, B. R. and Marshall, D. B., A critical evaluation of indentation techniques for measuring fracture toughness: I, direct crack measurements. *J. Am. Ceram. Soc.*, 1981, **64**, 533–538.
28. Marshall, D. B., Toma, T. and Evans, A. G., A simple method for determining elastic-modulus-to-hardness ratios using Knoop indentation measurements. *J. Am. Ceram. Soc.*, 1982, **65**, C175–C176.
29. Kim, Y. W., Mitomo, M. and Hirosaki, N., *R*-curve behavior of sintered silicon nitride. *J. Mater. Sci.*, 1995, **30**, 4043–4048.
30. Kaliszewski, M. S., Behrens, G., Heuer, A. H., Shaw, M. C., Marshall, D. B., Dransmann, G. W., Steinbrech, R. W., Pajares, A., Guiberteau, F., Cumbrera, F. L. and Dominguez-Rodriguez, A., Indentation studies on Y_2O_3-stabilized ZrO_2: I, development of indentation-induced cracks. *J. Am. Ceram. Soc.*, 1994, **77**, 1185–1193.
31. Dransmann, G. W., Steinbrech, R. W., Pajares, A., Guilberteau, F., Dominguez-Rodriguez, A. and Heuer, A. H., Indentation studies on Y_2O_3-stabilized ZrO_2: II, toughness determination from stable growth of indentation-induced cracks. *J. Am. Ceram. Soc.*, 1994, **77**, 1194–1201.
32. Lawn, B. R., Evans, A. G. and Marshall, D. B., Elastic/plastic indentation damage in ceramics: the median/radial crack system. *J. Am. Ceram. Soc.*, 1980, **63**, 574–581.

33. Krause, R. F. Jr., Rising fracture toughness from the bending strength of indented alumina beams. *J. Am. Ceram. Soc.*, 1988, **71**, 338–343.
34. Garvie, R. C. and Nicholson, P. S., Phase analysis in zirconia systems. *J. Am. Ceram. Soc.*, 1972, **67**, 303–305.
35. Reed-Hill, R. E., *Physical Metallurgy Principles*. D. Van Nostrand, New York, 1973 p. 318.
36. Li, J.-F. and Watanabe, R., Fracture Toughness of Al_2O_3-particle-dispersed Y_2O_3-partially stabilized zirconia. *J. Am. Ceram. Soc.*, 1995, **78**, 1079–1082.
37. Evans, A. G. and Cannon, R. M., Toughening of brittle solids by martensitic transformation. *Acta Metall.*, 1986, **34**, 761–800.
38. Esper, F. J., Friese, K. H. and Geier, H., *Advances in Ceramics, Vol. 12* ed. N. Claussen, M. Rühle and A. Heuer, Am. Ceram. Soc., Westerville, OH, 1984. p. 528.
39. Kendall, K., Alford, N.McN. and Birchall, J. D., *Proceedings of Materials Research Society Symposia, Vol. 78*, ed. P. F. Becher, M. V. Swain and S. Somiya, Mater. Res. Soc., Pittsburgh, PA, 1987, p. 189.
40. Freim, J. and McKittrick, J., Modeling and fabrication of fine-grain alumina-zirconia composites produced from nanocrystalline precursors. *J. Am. Ceram. Soc.*, 1998, **81**, 1773–1780.
41. Becher, P. F., Alexander, A. B., Bleier, A., Waters, S. B. and Warwick, W. H., Influence of ZrO_2 grain size and content on the transformation response in the Al_2O_3-ZrO_2 (12 mol% CeO_2) system. *J. Am. Ceram. Soc.*, 1993, **76**, 657–663.
42. Engineering Property Data on Selected Ceramics, Vol. 3. Single Oxide, Metals, and Ceramics, Information Center, Battelle Columbus Laboratories, Columbus, OH, 1981.
43. Whittemore, O. J. Jr. and Ault, N. N., Thermal expansion of various ceramic materials to 1500 °C. *J. Am. Ceram. Soc.*, 1957, **39**, 443–444.